Fuzzy Neural Network Control for Vehicle Stability Utilizing Magnetorheological Suspension System

Miao Yu[1,*], S. B. Choi[2], X. M. Dong[1] and C. R. Liao[1]

[1]*Key Lab of Opto-Electronic Technology & System, Education Ministry Department of Optoelectronic Engineering, Chongqing University, 400044 Chongqing, China*

[2]*Department of Mechanical Engineering, Smart Structures and Systems Laboratory Inha University, Incheon 402–751, Korea*

ABSTRACT: This paper presents the stability of a passenger vehicle system featuring magnetorheological (MR) suspensions. As a first step, MR damper is devised and its field-dependent damping force is experimentally evaluated. A full-car model equipped with the MR damper is established by considering roll motion which is directly related to the vehicle stability. A fuzzy neural network controller (FNNC) incorporated with the self-learn knowledge is then formulated in order to improve vehicle stability. In addition, in order to eliminate adverse effect of the system coupling, nonlinearity and time delay a correction component for updating the weighting matrix and adjusting controller outputs is designed. Both computer simulation and road test are undertaken in order to demonstrate the effectiveness of the proposed control method. The control results obtained in this work indicate that the proposed control scheme with the MR suspension can considerably improve the stability of vehicles with high performance in vibration isolation.

Key Words: fuzzy neural network control, magnetorheological damper, vehicle stability, vibration control, road test.

INTRODUCTION

It is well known that roll motion of vehicle system is one of very important criteria to evaluate vehicle stability. A moderate roll motion of the vehicles keeps the stability from capsizing. However, excessive roll motion is also a problem – giving a ride with uncomfortably high accelerations and rapid rocking movements. Thus, in traditional vehicle suspension roll stability needs to be compromised between these two extremes. If the primary suspension is designed to be soft, the vibrations in the vehicle can be reduced, but the vehicle may not be stable during maneuvers. On the other hand, if the suspension is optimized to achieve robust stability, the passenger is subject to excessive vibrations and may feel uncomfortable. In order to resolve this problem, intelligent suspension systems associated with electrorheological (ER) or magnetorheological (MR) dampers have been proposed and investigated by numerous researchers.

The controllable dampers have been developed based on ER/MR fluids (Carlson et al., 1995; Wereley and Pang, 1998; Gavin, 1998; Milecki, 2001; Lindler et al., 2000; Gordaninejad and Kelso, 2000, Dogruer et al., 2003). Some significant works have been done focusing on dynamic characteristics of ER/MR dampers (Miller et al., 1995; Spencer et al., 1997; Wereley et al., 1999; Sims et al., 2000). It is known that from the practical view point MR damper is more popular than ER damper owing to its lower voltage requirement and pollution insensitivity. Many investigators have proposed MR damper for the vehicle suspension system. In order to optimally control the dynamics of the vehicle, several semi-active control methods have been proposed. Ahmadian and Christopher (2000) constructed a quarter car suspension system model using MR damper and investigated the performance of three semi-active control strategies: skyhook control, ground-hook control, and hybrid control. Song et al. (2003) presented two alternative implementations of skyhook control, named 'skyhook function' and 'no-jerk skyhook,' for reducing the sharp increase in damping force. Those work were based on the two DOF model of vehicle which ignored the coupling of four wheels. Choi et al. (2002) have developed a H∞ control scheme for a full-vehicle suspension system featuring MR dampers, and evaluated the control performance under various road conditions through the hardware-in-the-loop simulation (HILS) methodology. However, this controller requires many

*Author to whom correspondence should be addressed.
E-mail: yumiao@cqu.edu.cn
Figures 2–4 and 10–17 appear in color online: http://jim.sagepub.com

1045-389X/09/04 0457–10 $10.00/0 DOI: 10.1177/1045389X08091972

feedback state variables that cannot easily achieved in practice. Recently, for the MR suspension system some intelligent control strategies such as fuzzy logical control, adaptive control and neural network control (Song et al., 2003; Guo et al., 2004; Liu et al., 2004, Wang and Liao, 2005, Xu, 2003) were introduced. A neural network *b*ased fuzzy control approach was also proposed by Nima Eslaminasab et al. (2007) to improve ride comfort and road handling of heavy vehicles using semi-active dampers via numerical simulation without involving in modeling and inverse modeling of MR damper. These control schemes are effective to vibration attenuation. However, most of them are formulated based on the two degree freedom model of a car without considering the coupling of four wheels and vehicle stability.

Consequently, the main contribution of this work is to present an effective intelligent control scheme to improve both ride comfort and vehicle stability. In order to achieve this goal, a cylindrical MR damper is devised and its field-dependent damping force is experimentally evaluated. A full-car model equipped with the proposed MR damper is then formulated by considering roll motion. A fuzzy neural network controller (FNNC) is designed in order to improve roll stability in which the self-learn knowledge via genetic algorithm (GA) and fuzzy associative memory neural network (FAMNN) are adopted. The effectiveness of the proposed control method is demonstrated via both computer simulation and road test. In addition, the proposed method is compared with the conventional sky-hook controller by presenting pitch roll angular acceleration as well as vertical acceleration in frequency domain.

MODEL OF FULL CAR WITH MR DAMPERS

MR Damper

The schemetic configuration of a controllable MR damper proposed in this work is shown in Figure 1. The damper has a twin-tube structure opearated on the basis of mixed mode (shear and flow mode). The MR damper is divided into the left and right chamber by the piston, and it is fully filled with the MR fluid. When the piton moves from left to right, the MR fluid flows through the damping path (the gap) between the inner cylinder and the piston. The magnet field exists in the gap perpendicular to the motion direction of the MR fluid once the input current is applied to the coil. The apparent viscosity of the MR fluid in the gap is changed under the supplied magnet field and the pressure drop across the piston. This leads to the controllable damping force of the proposed MR damper.

By considering the required damping force of the test vehicle, the pricipal design parameters of the MR damper are determined. Four MR dampers are designed and manufactured for two front suspensions and for two rear suspensions (refer to Figure 2). The dampers are manufactured by the Center for Smart Structure Research of Chongqing University. The diameter of the outer/inner cylinder is 50 mm and 48 mm, respectively which is same for the front and rear dampers. The compressed length of the fornt one is 330 mm, and it reaches 508 mm when it is extended. The rear damper is 50 mm shorter than the front one because of the vehicle's structure.

Because of the inherent hysteretic behaviors of the MR damper it is very difficult to directly determine input current to achive desired damping force. Among several models to predict the field-dependent hysteretic behaviors, the polynomial mode is adopted in this work which was proposed by Choi et al. (2001). This model can easily determine the input current according to desirable damping force and relative velocity. In this model, the hysteresis loop is divided into two regions: positive acceleration (lower loop) and negative acceleration (upper loop), which can be fitted by the polynomial

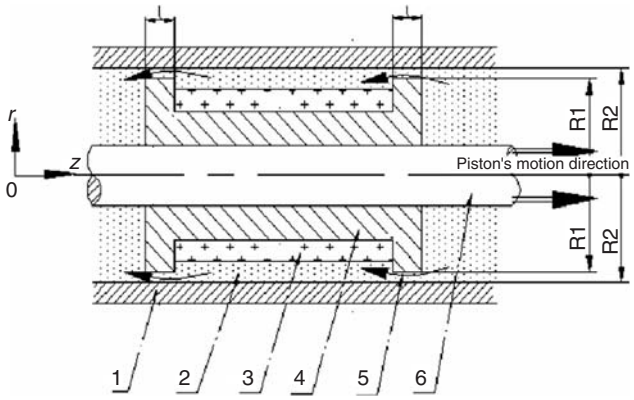

Figure 1. *Configuration of the proposed mixed mode MR damper.*

Figure 2. *Photograph of the manufactured MR damper.*

with the power of piston velocity. Thus the damping force of the MR damper can be written:

$$f_{\mathrm{MR}} = \sum_{i=0}^{7} a_i v^i \quad \text{for } i = 1, 2, \ldots, 7, \tag{1}$$

where v^i means the i order power of piston velocity, and the efficient a_i can be linearly approximated with respect to the input current I as follows:

$$a_i = b_i + c_i I \quad i = 1, 2, \ldots, 7.$$

Therefore, the damping force can be expressed by

$$f_{\mathrm{MR}} = \sum_{i=0}^{7} (b_i + c_i I) v^i. \tag{2}$$

In the above, the coefficient b_i and c_i are obtained from the fitness of data. The specific values of b_i and c_i used in this work are listed in Table 1.

In order to verify the obtained polynomial model the measured and simulated results are compared under four operating conditions. Figure 3 present plots for damping force versus displacement and for damping force versus velocity at 0.3 m/s, and Figure 4 plots for damping force versus displacement and for damping force versus velocity at 0.6 m/s Once the piston velocity and the

Table 1. The coefficients b_i and c_i of the polynomial model.

Positive acceleration				Negative acceleration			
b_0	−278.45	c_0	−368.23	b_0	−143.25	c_0	−578.29
b_1	150.74	c_1	489.57	b_1	131.58	c_1	650.47
b_2	1.87	c_2	27.88	b_2	−7.55	c_2	−58.96
b_3	−12.45	c_3	−43.86	b_3	−18.57	c_3	−57.62
b_4	−1.08	c_4	−15.78	b_4	0.97	c_4	12.36
b_5	1.98	c_5	3.89	b_5	2.89	c_5	4.67
b_6	−4.89e-8	c_6	5.48e-7	b_6	−8.46e-8	c_6	−4.35e-7
b_7	−3.32e-7	c_7	−4.33e-7	b_7	−3.79e-7	c_7	−9.68e-7

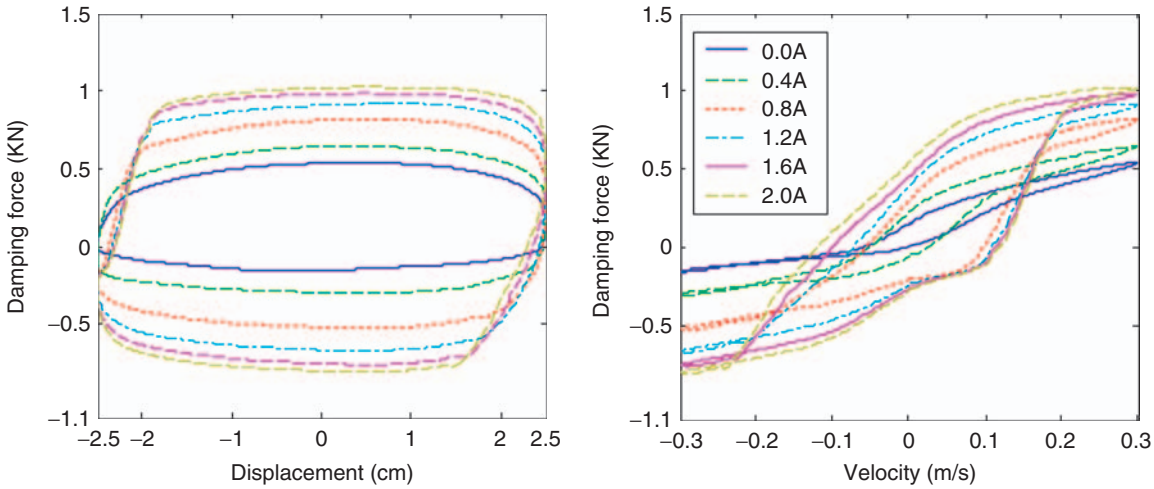

Figure 3. *Plots for damping force vs displacement and for damping force vs velocity at 0.3 m/s.*

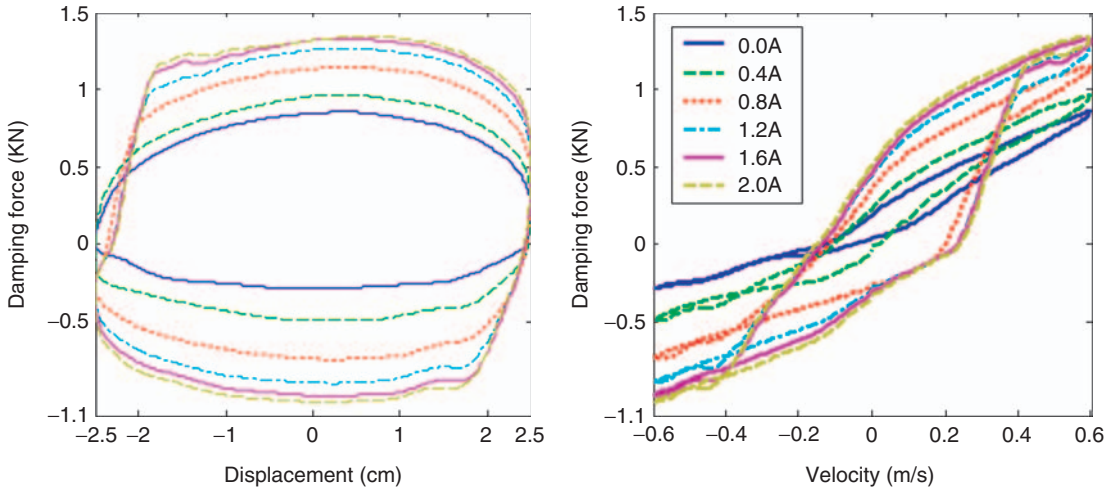

Figure 4. *Plots for damping force vs displacement and for damping force vs velocity at 0.6 m/s.*

desired damping force are known, the control input current is determined from the following equation.

$$I = \frac{f_{\mathrm{MR}} - \sum_{i=0}^{7} b_i v^i}{\sum_{i=0}^{7} c_i v^i}, \tag{3}$$

where I is the input current for the MR damper and f_{MR} is the control damping force which is to be determined by the control strategy. Figure 5 presents a block-diagram for realization of Equation (3). The controller to be designed in nest section calculates the damping forces according to inputs of sensors. Then the actual control curr-ents are determined by the inverse model of Equation (3) according to relative velocity of the MR damper and damping force determined by control scheme. During control process in simulation, the MR damper model depicted in Equation (2) considering the hysteresis of the MR damper is needed. It is noted that in the field test the real MR damper replaces the damper model.

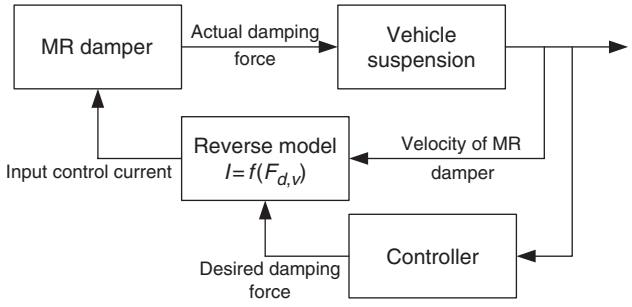

Figure 5. *MR damper's model applied to control system.*

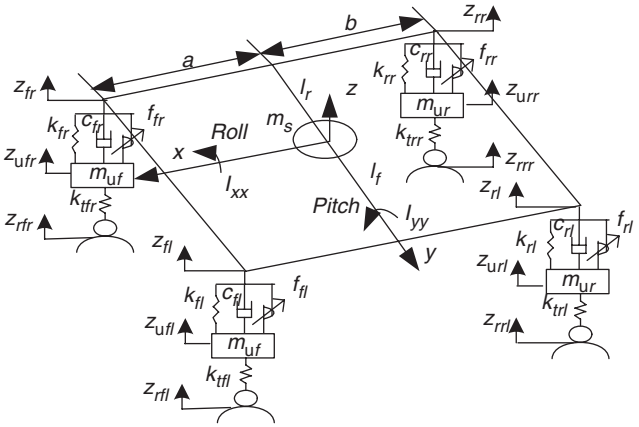

Figure 6. *Model of full car.*

Model of Full Car

The dynamic model of the full car equipped with MR dampers is shown in Figure 6. As shown in the model, vertical motion, roll motion, and pitch motion are considered to investigate both ride comfort and vehicle stability. The governing equations of motion of the full car is derived as follows (Dong et al., 2005):

$$\begin{aligned} M_{\mathrm{s}}\ddot{z} &= -K_{fl}(z_{fl} - z_{\mathrm{u}fl}) + u_{fl} - K_{fr}(z_{fr} - z_{\mathrm{u}fr}) + u_{fr} \\ &\quad - K_{rl}(z_{rl} - z_{\mathrm{u}rl}) + u_{rl} - K_{rr}(z_{rr} - z_{\mathrm{u}rr}) + u_{rr} \end{aligned} \tag{4}$$

$$\begin{aligned} I_{yy}\ddot{\theta} &= K_{fl}(z_{fl} - z_{\mathrm{u}fl})a + u_{fl}a + K_{fr}(z_{fr} - z_{\mathrm{u}fr})a \\ &\quad - u_{fr}a - K_{rl}(z_{rl} - z_{\mathrm{u}rl})b + u_{rl}b \\ &\quad - K_{rr}(z_{rr} - z_{\mathrm{u}rr})b + u_{rr}b \end{aligned} \tag{5}$$

$$\begin{aligned} I_{xx}\ddot{\varphi} &= -K_{fl}(z_{fl} - z_{\mathrm{u}fl})l_f + u_{fl}l_f + K_{fr}(z_{fr} - z_{\mathrm{u}fr})l_r \\ &\quad - u_{fr}l_r - K_{rl}(z_{rl} - z_{\mathrm{u}rl})l_f + u_{rl}l_f \\ &\quad + K_{rr}(z_{rr} - z_{\mathrm{u}rr})l_r - u_{rr}l_r \end{aligned} \tag{6}$$

$$\begin{aligned} M_{\mathrm{u}fl}\ddot{z}_{\mathrm{u}fl} &= K_{fl}(z_{fl} - z_{\mathrm{u}fl}) - u_{fl} - K_{tfl}(z_{\mathrm{u}fl} - z_{rfl}) \\ M_{\mathrm{u}fr}\ddot{z}_{\mathrm{u}fr} &= K_{fr}(z_{fr} - z_{\mathrm{u}fr}) - u_{fr} - K_{tfr}(z_{\mathrm{u}fr} - z_{rfr}) \\ M_{\mathrm{u}rl}\ddot{z}_{\mathrm{u}rl} &= K_{rl}(z_{rl} - z_{\mathrm{u}rl}) - u_{rl} - K_{trl}(z_{\mathrm{u}rl} - z_{rrl}) \\ M_{\mathrm{u}rr}\ddot{z}_{\mathrm{u}rr} &= K_{rr}(z_{rr} - z_{\mathrm{u}rr}) - u_{rr} - K_{trr}(z_{\mathrm{u}rr} - z_{rrr}). \end{aligned} \tag{7}$$

In the above, a, b, l_r, l_f is the distance of each corner to the center of sprung mass, M_{s} is the sprung mass and M_{u} is the unsprung mass. z_{fl}, z_{fr}, z_{rl}, z_{rr} is the displacement of the sprung mass in four corners, respectively, and $z_{\mathrm{u}fl}$, $z_{\mathrm{u}fr}$, $z_{\mathrm{u}rl}$, $z_{\mathrm{u}rr}$ is the displacement of each unsprung mass. K_{fl}, K_{fr}, K_{rl}, K_{rr} is the stiffness of each spring and I_{xx}, I_{yy} is the moment of inertia for pitch and roll motion of vehicle body. θ and φ is the pitch and roll angle, and u_{fl}, u_{fr}, u_{rl}, u_{rr} is the damping force of four MR damper and given as follows:

$$\begin{aligned} u_{fl} &= -c_{fl}(\dot{z}_{fl} - \dot{z}_{\mathrm{u}fl}) + f_{fl}\mathrm{sign}(\dot{z}_{fl} - \dot{z}_{\mathrm{u}fl}) \\ u_{fr} &= -c_{fr}(\dot{z}_{fr} - \dot{z}_{\mathrm{u}fr}) + f_{fr}\mathrm{sign}((\dot{z}_{fr} - \dot{z}_{\mathrm{u}fr}) \\ u_{rl} &= -c_{rl}(\dot{z}_{rl} - \dot{z}_{\mathrm{u}rl}) + f_{rl}\mathrm{sign}(\dot{z}_{rl} - \dot{z}_{\mathrm{u}rl}) \\ u_{rr} &= -c_{rr}(\dot{z}_{rr} - \dot{z}_{\mathrm{u}rr}) + f_{rr}\mathrm{sign}(\dot{z}_{rr} - \dot{z}_{\mathrm{u}rr}), \end{aligned} \tag{8}$$

where c_{fl}, c_{fr}, c_{rl}, c_{rr} is system damp coefficient of each suspension and f_{fl}, f_{fr}, f_{rl}, f_{rr} is the damping force f_{MR} of each damper which can be calculated by Equation (2). And $sign(x)$ is a signum function.

FUZZY NEURAL NETWORK CONTROLLER

It is known that control performance of model based control scheme heavily depends on the accuracy of the dynamic model. In real field, the dynamic model of the MR suspension system is very complex and includes nonlinearities. Therefore, an intelligent controller which

is less sensitive to the model accuracy may bring good control performance for the vehicle suspension system. In this work, a model-free FNNC algorithm is employed to design a controller for achieving roll control. The fuzzy rules and membership functions of the FNNC are selected by FAMNN from training data which is presented by Kosko (1987). The training data is generated by GA, which is presented by John Holland (1962).

In order to reduce roll and vibration of the vehicle, the input state vector of the fitness function and FAMNN is defined as $X = [\varphi, \theta, Z]$. The output state vector is defined as follows:

$$F = [F_{fl}, F_{fr}, F_{rl}, F_{rr}].$$

On the other hand, the fitness function is selected as follows:

$$Fit = \sqrt{\frac{1}{T}\int_0^T \theta^2 \mathrm{d}t} + \sqrt{\frac{1}{T}\int_0^T \varphi^2 \mathrm{d}t} + \sqrt{\frac{1}{T}\int_0^T Z^2 \mathrm{d}t}. \quad (9)$$

Figure 7 presents the block diagram for the generation of knowledge base system. With the road input and damping force for the four MR dampers being supplied, the full-car model calculates the motion of the suspension and vehicle. Then, the GA searches out the best damping force of the MR damper that minimizes the fitness function in every sampling period. A series of such damping force and system state are stored as teaching signals for FAMNN. The error of the teaching signals and FAMNN's outputs is used to adjust the knowledge base. As a feedback, the knowledge base will affect the FAMNN's output until the error is small enough.

Since pitch angle θ and roll angle φ are small enough, the displacement of each corner can be calculated as follows:

$$z_{fl} = z - a\theta + l_f\varphi, \quad z_{fr} = z - a\theta - l_r\varphi,$$

$$z_{rl} = z + b\theta + l_f\varphi, \quad z_{rr} = z + b\theta - l_r\varphi$$

$$\varphi = \frac{z_{fl} - z_{fr}}{l_f + l_r} = \frac{z_{rl} - z_{rr}}{l_f + l_r}, \quad \theta = \frac{z_{fl} - z_{rl}}{a + b} = \frac{z_{fr} - z_{rr}}{a + b},$$

$$z \approx \frac{z_{fl} + z_{rl} + z_{fr} + z_{rr}}{4}.$$

The architecture of the FAMNN is proposed and shown in Figure 8. The FAMNN has two layers; $X^k = [\varphi^k, \theta^k, Z^k]$ is the kth input vector of FAMNN and $F^k = [F^k_{fl}, F^k_{fr}, F^k_{rl}, F^k_{rr}]$ is the kth output vector of FAMNN. In this work, $X^k = [x^k_1, x^k_2, \ldots, x^k_{3n}]$ and $F^k = [f^k_1, f^k_2, \ldots, f^k_{4n}]$ $(n = 7)$ are fuzzified in $[-7,7]$.

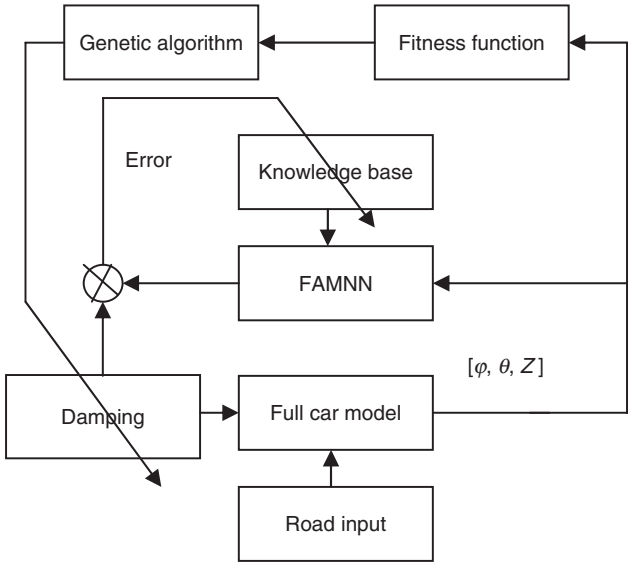

Figure 7. *Block diagram for generation of knowledge base.*

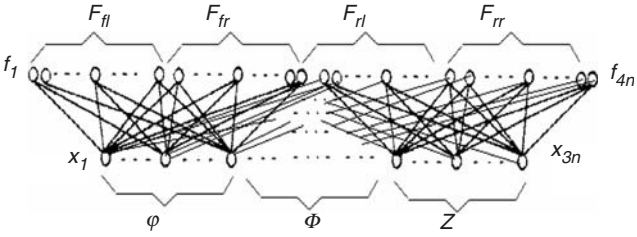

Figure 8. *Scheme of FAMNN.*

Thus, X^k is a 21D input vector and F^k is a 28D output vector. All vectors are defined as follows:

$$\varphi^k = [x^k_1, x^k_2, \ldots, x^k_n], \quad \theta^k = [x^k_{n+1}, x^k_{n+2}, \ldots, x^k_{2n}],$$

$$Z^k = [x^k_{2n+1}, x^k_{2n+2}, \ldots, x^k_{3n}],$$

$$F^{fl}_k = [f^k_1, f^k_2, \ldots, f^k_n], \quad F^k_{fr} = [f^k_{n+1}, f^k_{n+2}, \ldots, f^k_{2n}],$$

$$F^k_{rl} = [f^k_{2n+1}, f^k_{2n+2}, \ldots, f^k_{3n}],$$

$$F^k_{rr} = [f^k_{3n+1}, f^k_{3n+2}, \ldots, f^k_{4n}].$$

These fuzzy rules can be expressed by the following statement:

Ri: IF (X is X^i) Then the system output is F^i

The above statement can be also described as follows:

$$Ri: \quad F^k = W^k \circ X^k. \quad (10)$$

In the above, '$\circ$' means max–min operation. W^k is the connection weight matrix. It can be obtained via Hebb learning rules (Hebb, 1949). $w^k_{i,j}, (i = 1, \ldots, 21, j = 1, \ldots, 28)$ is the connection weight of input cell i and output cell j. $E^k = F^k - \bar{F}^k = [e^k_1, e^k_2, \ldots, e^k_{4n}]$, $(n = 7)$ is defined as the error of

the damping force calculated by FAMNN and GA. FAMNN will change W^k to build knowledge base according to $E^k = F^k - \bar{F}^k = [e_1^k, e_2^k, \ldots, e_{4n}^k]$, $(n = 7)$. The change is given by

$$w_{i,j}^{k+1} = w_{i,j}^k + \overset{p}{\underset{1}{\vee}}(x_i^k \wedge (e_j^k \cdot f_j^k)), \quad (k = 1, \ldots, 21, j = 1, \ldots, 28). \tag{11}$$

In the above, $\vee$ means max operation, $\wedge$ means min operation.

After the knowledge base is obtained by off-line training, it can be used in the fuzzy controller realization and will be updated online. Figure 9 presents a block diagram for the proposed control system. At the time of k, the output of controller $U(k)$ is given by

$$U(k) = W^k \circ X^k. \tag{12}$$

Because of the time delay of the system τ, the controller output will be corrected. If the correction matrix is A, the correction value will be:

$$P(k) = A \circ X^k. \tag{13}$$

At the time of $k - \tau$, controller output can be updated as follow:

$$U'(k - \tau) = U(k - \tau) + P(k). \tag{14}$$

The updated weight matrix of the time of $k - \tau$ is given by $W'^{k-\tau} = X^{k-\tau} \wedge U'(k - \tau)$.

And the weight matrix of next time is given by

$$W^{k+1} = [W^k \wedge (1 - W^{k-\tau})] \vee W'^{k-\tau} \tag{15}$$

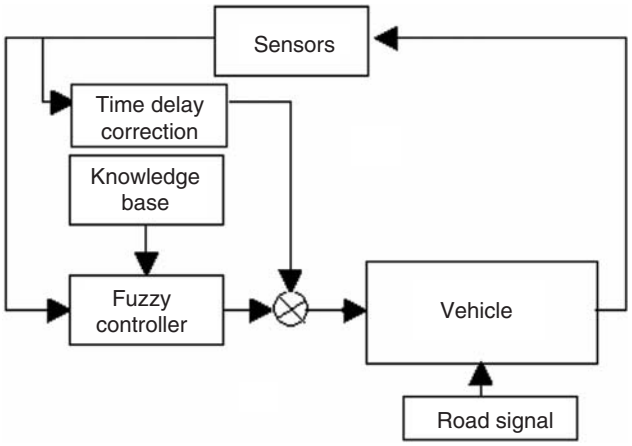

Figure 9. *Block diagram for the proposed Fuzzy Neural Network Control System.*

Thus, the controller output of next time is expressed as follows:

$$U(k + 1) = W^{k+1} \circ X^k. \tag{16}$$

In order to derive an accurate control output force for this control system, the weighted average (Min–Max) method is employed to defuzzify the fuzzy variables. The fuzzy intelligent controller output can be described as:

$$u = K_u \frac{\sum \mu_i(U_i) \cdot U_i}{\sum \mu_i(U_i)}, \tag{17}$$

where, μ_i represents the weight of the corresponding rules activated, U_i is the resulting fuzzy control values of the corresponding fuzzy rules, and K_u is the output proportion coefficient.

CONTROL RESULTS AND DISCUSSION

Before evaluating control performance via the road test, computer simulation is undertaken. The road roughness is chosen by Class D represented by a power spectral density function according to ISO 8606 (1995). The vehicle velocity u_0 is set by 11.11 m/s. The road input of the four wheels can be described as follows:

$$\dot{z}_{rfl} = -2\pi f_0 z_{rfl} + 2\pi\sqrt{G_0 u_0} w_{rfl},$$
$$\dot{z}_{rfr} = -2\pi f_0 z_{rfr} + 2\pi\sqrt{G_0 u_0} w_{rfr}$$
$$\dot{z}_{rrl} = -2\pi f_0 z_{rrl} + 2\pi\sqrt{G_0 u_0} w_{rrl},$$
$$\dot{z}_{rrr} = -2\pi f_0 z_{rrr} + 2\pi\sqrt{G_0 u_0} w_{rrr}.$$

In the above equation, G_0 is the coefficient of road roughness (m^3/c), w is Gaussian white noise and f_0 is the lower cutoff frequency of 0.01 Hz. The nominal parameters used for computer simulations are given in Table 2.

Figures 10–12 present control responses obtained from computer simulation. It can be seen that MR suspension employing FNNC reduces the pitch, roll,

Table 2. Simulation parameters of the test car.

Parameter	Value	Parameter	Value
m_s (Kg)	745.2	b (m)	1.2319
m_{uf} (Kg)	25.35	l_f (m)	0.6490
m_{ur} (Kg)	34.4	l_r (m)	0.6280
I_{xx} (Kgm^2)	375.2	K_{sf} (N/m)	17,000
I_{yy} (Kgm^2)	768.8	K_{sr} (N/m)	22,000
a (m)	1.1161	K_t (N/m)	200,000

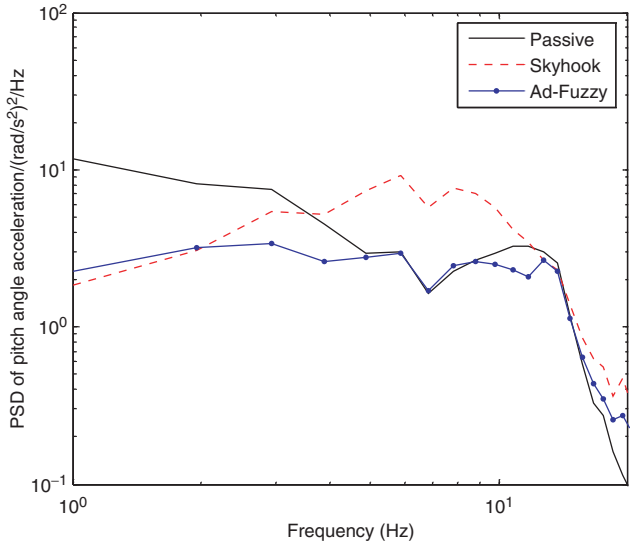

Figure 10. *Pitch acceleration response (simulation).*

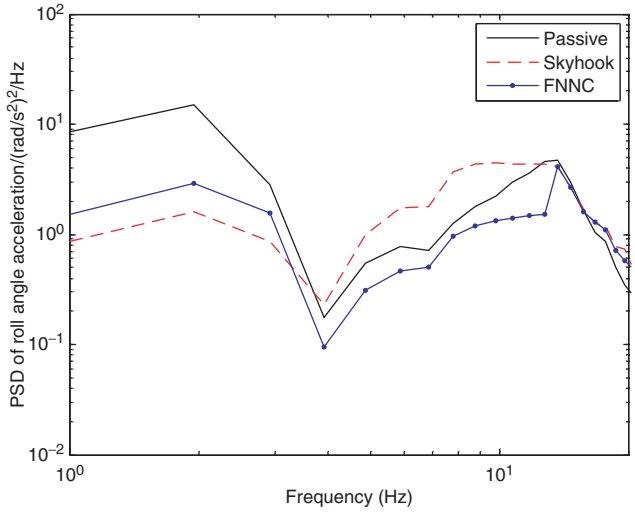

Figure 11. *Roll acceleration response (simulation).*

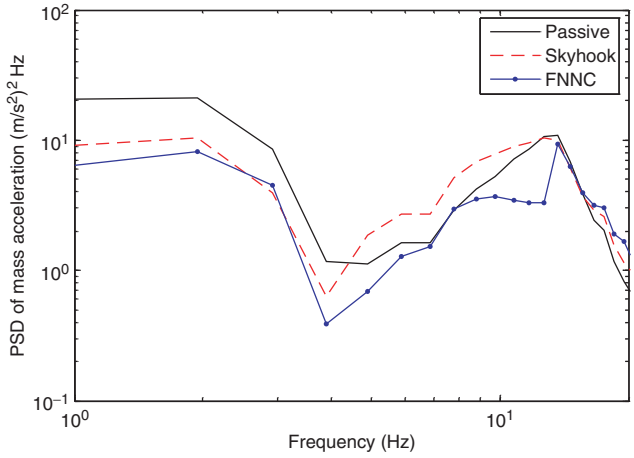

Figure 12. *Vertical acceleration response (simulation).*

and vertical acceleration of car body compared to the passive suspension up to the second resonance frequency of 10.3 Hz. However, it is observed that control performance is degraded at high frequency region above the second resonance frequency. This is because the semi-active MR dampers cannot supply enough energy to such high resonance modes. Because human body is not sensitive to the vibration beyond 12.5 Hz, the FNNC can achieve good roll ability in weighted root mean square (WRMS) value with weighted average in frequency domain. For the comparative study on control performances of the FNNC, a traditional sky-hook control strategy of the MR suspension is also evaluated. It is obviously seen that the proposed FNNC is better than the sky-hook controller in terms of ride comfort and vehicle stability.

As a second step for control performance evaluation, the road test is undertaken. The semi-active suspension control system of a MAZDA 323 car equipped with the MR dampers is set up and road tests are conducted. Control strategy is downloaded into dSPACE modular system from Matlab/Simulink software after the parameters are optimized. The dSPACE system is fastened in car's luggage compartment and employed to control the four MR dampers respectively (refer to Figure 13(a)). Four LVDT and one tiled-angle sensors are used to measure the deflection at various points on the car as the feedback signals for the controller input (Figure 13(b) and (c)). A 3D accelerometer (B&K Co.) is placed on driver's seat to calculate WRMS values (Figure 13(d)). Every seat has a passenger to hold the vehicle's balance. According to ISO2631, test car with half load is driven on Class D road along a stretch of straight road in constant vehicle speed of 11.11 m/s (refer to Figure 14). The accelerations of the body frame are sampled with low-pass cut-off frequency of 100 Hz and sampling frequency of 200 Hz. Every time the acquired data is divided into 25 sections, and each section has 1024 point. Power spectrum density (PSD) of each sampling data is calculated by 1024-point FFT with an average of 25 sections. In order to discuss the performance of the proposed FNNC, a conventional sky-hook controller is also utilized in the test. Figures 15–17 present control responses obtained from the road test. It is clearly observed that pitch motion, roll motion, and vertical motion are effectively reduced by activating the proposed FNNC. In addition, it is demonstrated that the proposed FNNC produces better control performance than the conventional sky-hook controller. Compared to simulation, the similar conclusion can be also drawn. Due to the difference between actual geometry parameters and simulation geometry, there are some discrepancy measured and numerical results.

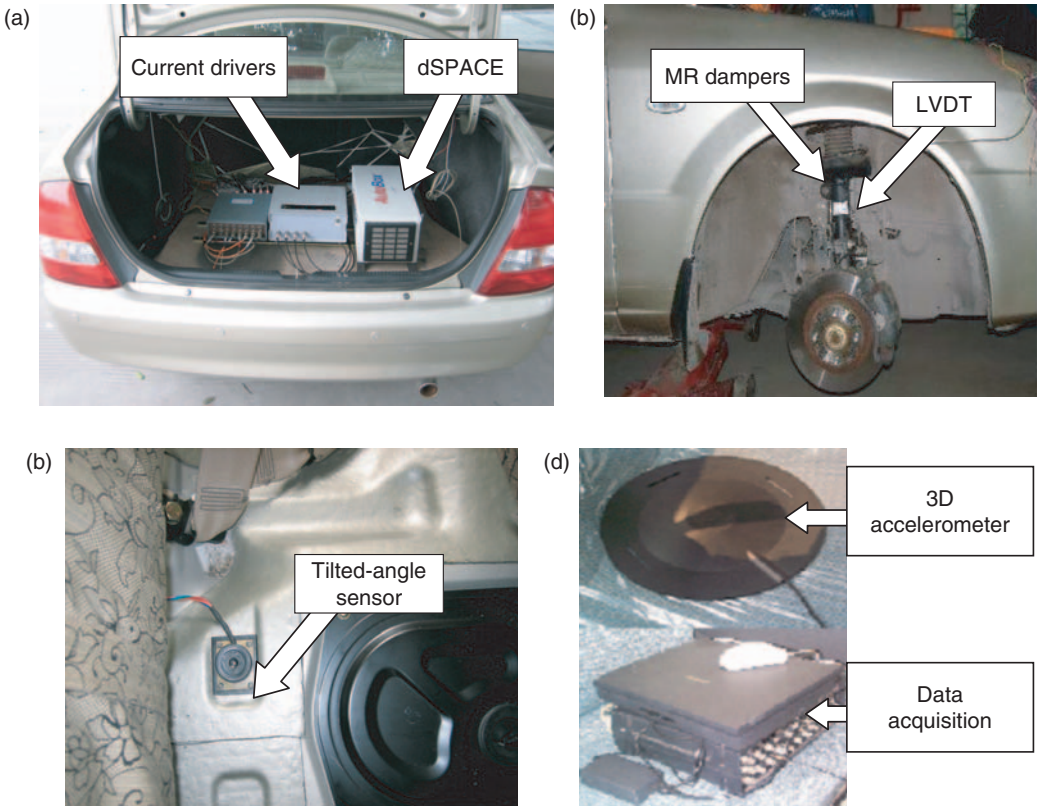

Figure 13. *Setup of the test car: (a) control system; (b) installation of MR dampers and LVDT; (c) tilted-angle sensor installed on vehicle's body and (d) evaluation system.*

Figure 14. *The car testing on the road with profile Class D.*

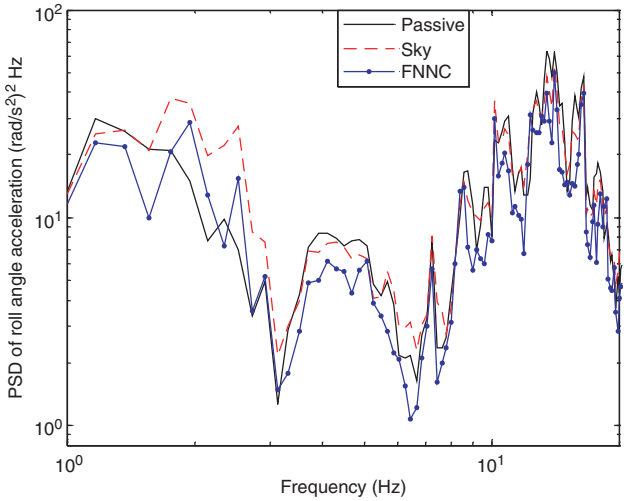

Figure 15. *Pitch acceleration response (measured).*

CONCLUSION

In this work a FNNC was developed and experimentally realized for MR suspension vehicle in order to enhance ride comfort and vehicle stability. A cylindrical MR damper was manufactured and its hysteretic behaviors were identified using the polynomial model. A full-car model equipped with the proposed MR damper was formulated and a FNNC was designed by integrating the self-learn knowledge base. Both computer simulation and road test were undertaken in order to demonstrate the effectiveness of the proposed control method. The pitch motion, roll motion, and vertical motion was significantly reduced by activating the

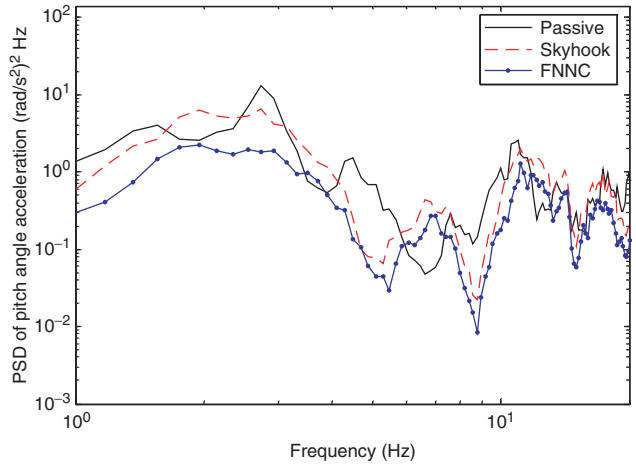

Figure 16. *Roll acceleration response (measured).*

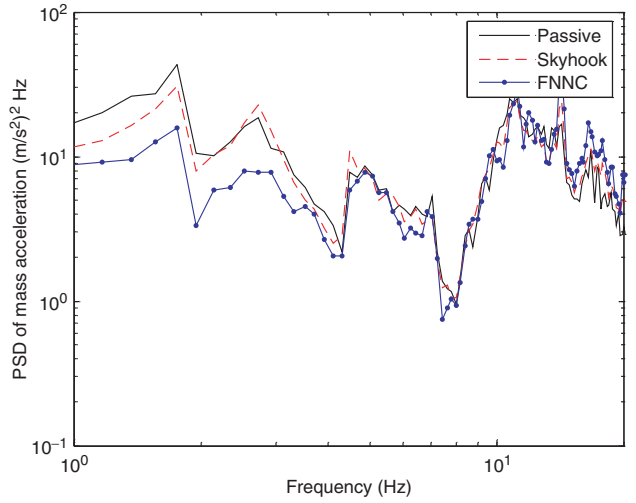

Figure 17. *Vertical acceleration response (measured).*

proposed control strategy. The results obtained in this work clear indicate that the proposed control scheme with the MR suspension can improve both ride comfort and stability of vehicles.

ACKNOWLEDGMENT

This work was supported by the National Natural Science Foundation of China (60404014, 60574074). This support is gratefully acknowledged.

REFERENCES

Ahmadian, M. and Christopher a.P. 2000. "A Quarter-Car Experimental Analysis of Alternative Semi-active Control Methods," *Journal of Intelligent Material Systems and Structures*, 11(8):604–612.

Ahmadian, M., Song, X. and Southward, S.C. 2004. "No-Jerk Skyhook Control Methods for Semiactive Suspension," *ASME Journal of Vibration and Acoustics*, 126(4):580–584.

Carlson, J.D. and Catanzarite et al. 1995. "Commercial Magneto-rheological Fluid Devices," *International Journal of Modern Physics B*, 10(23–24):2857–2865.

Choi, S.B., Lee, H.S. and Park, Y.P. 2002. "$H\infty$ Control Performance of a Full-Vehicle Suspension Featuring Magneto-rheological Dampers," *Vehicle System Dynamics*, 38(5):341–360.

Choi, S.B., Lee, S.K. and Park, Y.P. 2001. "A Hysteresis Model for the Field-dependent Damping Force of a Magneto-rheological Damper," *Journal of Sound and Vibration*, 245(2):375–383.

Dogruer, U., Gordaninejad, F., Evrensel, C.A. 2003. "A New Magneto-rheological Fluid Damper for High-mobility Multi-purpose Wheeled Vehicle (HMMWV)," In: *Proceedings of SPIE Conference on Smart Materials and Structures*, San Diego, March 2003.

Dong, X.M., Yu, M., Huang, S.L., Li, Z. and Chen, W.M. 2005. "Half Car Magneto-rheological Suspension System Accounting for Nonlinearity and Time Delay," *International Journal of Modern Physics B*, 19(7–9):1381–1387.

Eslaminasab, N., Biglarbegian, M., Melek, W.W., Golnaraghi, M.F. 2007. "A Neural Network Based Fuzzy Control Approach to Improve Ride Comfort and Road Handling of Heavy Vehicles using Semi-active Dampers," *International Journal of Heavy Vehicle Systems (IJHVS)*, 14(2):135–157.

Gavin, H.P. 1998. "Design Method for High-force Electrorheological Dampers," *Smart Materials and Structures*, 7(5):664–673.

Gordaninejad, F. and Kelso, S.P. 2000. "Fail-safe Magneto-rheological Fluid Dampers for Off-highway, High-payload Vehicles," *Journal of Intelligent Material Systems and Structures*, 11(5):395–406.

Guo, D.L., Hu, H.Y. and Yi, J.Q. 2004. "Neural Network Control for a Semi-Active Vehicle Suspension with a Magnetorheological Damper," *Journal of Vibration and Control*, 10(3):461–471.

Hebb, D. 1949. *The Organization of Behavior*, Wiley, New York.

Holland, J.H. 1962. "Outline for a Logical Theory of Adaptive Systems," *Journal of the Association for Computing Machinery*, 9:297–314.

Kosko, B. 1987. *Fuzzy Associative Memory Systems, Fuzzy Expert Systems*, Addison-Wesley, MA.

Lindler, J.E., Dimock, G.A. and Wereley, N.M. 2000. "Design of A Megnetorheological Automotive Shock Absorber," *Proc. SPIE*, 3985:426–437.

Liu, Y., Gordaninejad, F., Evrensel, C., Karakas, S. and Dogruer, U. 2004. "Experimental Study on Fuzzy Skyhook Control of a Vehicle Suspension System Using a Magneto-Rheological Fluid Damper," Industrial and Commercial Applications of Smart Structures Technologies, Proceedings of SPIE Conference on Smart Materials and Structures, Ed. by Jack H. Jacobs, 5388:338–347.

Milecki, A. 2001. "Investigation and Control of Magnetorheological Fluid Dampers," *International Journal of Machine Tools & Marufacture: Design, Research and Application*, 41:379–391.

Miller, L.R., Ahmadian, M., Nobles, C.M. and Swanson, D.A. 1995. "Modeling and Performance of an Experimental Active Vibration Isolator," *Trans. ASME, J. Vibration and Acoustics*, 117(3):272–278.

Sims, N.D., Peel, D.J., Stanway, R., Johnson, A.R. and Bullough, W.A. 2000. "The Electrorheological Long-stroke Damper: A New Modeling Technique with Experimental validation," *Journal of Sound and Vibration*, 229(2):207–227.

Song, X., Ahmadian, M. and Southward, S.C. 2003. "An Adaptive Semiactive Control Algorithm for Vehicle Suspension Systems," *ASME 2003 International Mechanical Engineering Congress and Exposition*, Washington, DC, November 16–21.

Spencer, B.F., Dyke, S.J., Sain, M.K. and Carlson, J.D. 1997. "Phenomenological Model for Magnetorheological Dampers," *Journal of Engineering Mechanics*, 123(3):230–238.

Wang, D.H. and Liao, W.H. 2005. "Modeling and Control of Magneto-rheological Fluid Dampers Using Neural Networks, *Smart Mater. Struct.*, 14(1):111–126.

Wereley, N.M. and Li Pang. 1998. "Nondimensional Analysis of Semi-Active Electrorheological and Magnetorheological Dampers Using Approximate Parallel Plate Models," *Smart Materials and Structures*, 7(5):732–743.

Wereley, N.M., Kamath, G.M. and Madhavan, V. 1999. "Hysteresis Modeling of Semi-active Magnetorheological Helicopter Dampers," *Journal of Intelligent Material Systems and Structures*, 10(8):624–633.

Xu, Z.-D., Shen, Y.-P. and Guo, Y.-Q. 2003. "Semi-active Control of Structures Incorporated with Magneto-rheological Dampers Using Neural Networks," *Smart Mater. Struct.*, 12(1):180–187.